Journal of Power Sources 247 (2014) 20–25

Contents lists available at ScienceDirect

Journal of Power Sources

journal homepage: www.elsevier.com/locate/jpowsour

Short communication

$Li[Li_{0.2}Mn_{0.54}Ni_{0.13}Co_{0.13}]O_2$–$MoO_3$ composite cathodes with low irreversible capacity loss for lithium ion batteries

Feng Wu [a,b], Zhao Wang [a], Yuefeng Su [a,b,*], Na Yan [a], Liying Bao [a,b], Shi Chen [a,b]

[a] School of Chemical Engineering and Environment, Beijing Institute of Technology, Beijing Key Laboratory of Environmental Science and Engineering, Beijing 100081, China
[b] National Development Center of High Technology Green Materials, Beijing 100081, China

HIGHLIGHTS

- $Li[Li_{0.2}Mn_{0.54}Ni_{0.13}Co_{0.13}]O_2$ is synthesized by a mixed oxalate method.
- MoO_3 is used to eliminate the large first-cycle irreversible capacity loss.
- The composite with 5 wt.% MoO_3 shows a good cycling stability.
- A nano-sized MoO_3 coating layer is obtained by high-energy ball milling process.

ARTICLE INFO

Article history:
Received 29 April 2013
Received in revised form
6 August 2013
Accepted 8 August 2013
Available online 19 August 2013

Keywords:
Lithium-ion battery
Lithium-rich
Cathode materials
Compositing
Irreversible capacity loss

ABSTRACT

To reduce the large first-cycle irreversible capacity loss of the Li-rich layered cathode material $Li[Li_{0.2}Mn_{0.54}Ni_{0.13}Co_{0.13}]O_2$, MoO_3 has been introduced by a simple high-energy ball milling process. The electrochemical properties of cathode material $Li[Li_{0.2}Mn_{0.54}Ni_{0.13}Co_{0.13}]O_2$ and the influences of different MoO_3 amount on its electrochemical properties are discussed in detail. The first charge–discharge dQ/dV curves suggest that the MoO_3 component provides additional sites for lithium ion insertion to compensate the lost Li sites caused by the simultaneous removal of Li^+ and O^{2-} during the activation of $Li[Li_{0.2}Mn_{0.54}Ni_{0.13}Co_{0.13}]O_2$. With increasing MoO_3 content from 0 wt.% to 20 wt.%, the first-cycle irreversible capacity loss of the composite decreases from 81.8 mAh g^{-1} to 1.2 mAh g^{-1}. The composite with 5 wt.% MoO_3 exhibits a good cycling stability with the discharge capacity of 242.5 mAh g^{-1} after 50 cycles, and the thickness of the MoO_3 coating layer on the surface of $Li[Li_{0.2}Mn_{0.54}Ni_{0.13}Co_{0.13}]O_2$ is about 3–4 nm. However, with the increase of the addition content of MoO_3, the cycling stability of the $Li[Li_{0.2}Mn_{0.54}Ni_{0.13}Co_{0.13}]O_2$–$MoO_3$ composite is decreased.

1. Introduction

Lithium ion batteries have attracted much attention for applications in automobiles and stationary power storage for its higher energy density compared to other rechargeable systems [1–3]. Developing high performance cathode materials is the critical technology for the development of advanced lithium ion batteries. The conventional cathode materials, such as $LiCoO_2$, $LiMn_2O_4$, $LiMn_{1/3}Ni_{1/3}Co_{1/3}O_2$, and $LiFePO_4$, cannot fully satisfy the energy density demanded of the electronic products, especially electric cars, because of the limited practical capacities [4–6]. In this regard, solid solution cathode materials between layered Li_2MnO_3 ($Li[Li_{1/3}Mn_{2/3}]O_2$) and $LiMO_2$ (M = Mn, Ni, and Co……) are promising as a high-voltage cathode material of lithium-ion batteries for applications in electric transportation, owing to the higher discharge capacity of 250 mAh g^{-1} [6–12].

However, these lithium-rich cathode materials exhibit a large irreversible capacity loss about 80 mAh g^{-1} in the first cycle, which limits their wide application. [13–15]. The irreversible capacity loss is attribute to the simultaneous removal of Li^+ and O^{2-} (as Li_2O) from the lattice of Li_2MnO_3 ($Li[Li_{1/3}Mn_{2/3}]O_2$) component on charging beyond the oxidation of the valence of the transition metal ions above +4, which leads to the elimination of oxygen ion vacancies in the first charge progress [6,14,16,17]. The vacancies lead to a decrease in the number of intercalation sites for lithium. In the subsequent discharge progress, not all the extracted lithium ions can insert back into the layered lattice [13–15].

* Corresponding author. School of Chemical Engineering and Environment, Beijing Institute of Technology, Beijing Key Laboratory of Environmental Science and Engineering, Beijing 100081, China. Tel.: +86 10 6891 8099; fax: +86 10 6891 8200.
E-mail address: suyuefeng@bit.edu.cn (Y. Su).

0378-7753/$ – see front matter © 2013 Elsevier B.V. All rights reserved.
http://dx.doi.org/10.1016/j.jpowsour.2013.08.031

To overcome this problem, some efforts such as surface modification with Al_2O_3, $AlPO_4$, $CoPO_4$ and TiO_2 [15,18–20], surface treatment with mild acids [17,21], have been done. The decrease in irreversible capacity loss can be attributed to the retention of some oxygen ion vacancies in the lattice after the first charge on surface modification [18]. However, because of impossibility to retain all the oxygen ion vacancies in the lattice completely after the first charge, these methods cannot eliminate the irreversible capacity loss completely. There are some efforts in some other way, such as compositing this solid solution cathode material with V_2O_5, $Li_4Mn_5O_{12}$ and LiV_3O_8 [22,23], coating a thick layer of electrochemical active delithiated oxides MnO_x [24]. However, the cyclic performance of the composite is not improved.

In this study, we have explored the possibility of compensating the irreversible capacity loss by providing additional Li^+ insertion sites through compositing the layered oxide $Li[Li_{0.2}Mn_{0.54}Ni_{0.13}Co_{0.13}]O_2$ ($0.6Li[Li_{1/3}Mn_{2/3}]O_2$–$0.4Li[Mn_{1/3}Ni_{1/3}Co_{1/3}]O_2$) with MoO_3. MoO_3 as the lithium-free insertion host can accommodate the lithium ions that could not insert back into the layered lattice after the first charge. XRD, SEM, TEM and the charge–discharge properties of the $Li[Li_{0.2}Mn_{0.54}Ni_{0.13}Co_{0.13}]O_2$–$MoO_3$ composite have been explored.

2. Experimental

2.1. Synthesis of the materials

$Li[Li_{0.2}Mn_{0.54}Ni_{0.13}Co_{0.13}]O_2$ was synthesized by a mixed oxalate method. The aqueous solution with nickel nitrate, manganese nitrate and cobalt nitrate was co-precipitated with ammonium oxalate aqueous solution by slowly pumping two solutions in a reaction tank, while the reaction solution was stirred vigorously with the pH value maintained at 7.0 using ammonia to obtain mixed oxalate precipitations. Precipitates were isolated by vacuum filtration and washed multiple times with distilled deionized water and dried in the vacuum oven at 80 °C for 12 h. The dried mixed oxalate precipitations were mixed with a required amount $LiNO_3$, and then preliminarily fired at 450 °C for 5 h in air. Afterward, the precursors were pressed into pellets and calcined at 900 °C for 12 h in air and naturally cooled to room temperature. The $Li[Li_{0.2}Mn_{0.54}Ni_{0.13}Co_{0.13}]O_2$–$MoO_3$ composite was prepared by high-energy ball milling $Li[Li_{0.2}Mn_{0.54}Ni_{0.13}Co_{0.13}]O_2$ with required amount of $(NH_4)_6Mo_7O_{24}\cdot 4H_2O$ and then heating the mixture in air at 600 °C for 2 h. The pure MoO_3 sample was also prepared by heating $(NH4)_6Mo_7O_{24}\cdot 4H_2O$ under the same conditions. All the raw materials of transition metal salts were of analytical purity grade.

2.2. Structure characterization

Powder X-ray diffraction (XRD) was performed on Rigaku Ultima IV–185 with Cu-Kα radiation between 10 and 90° 2θ at a scan rate of 8° 2θ/min to characterize the crystal structures of the synthesized materials. Field emission scanning electron microscopy (FESEM, FEI QUANTA 250) and high-resolution transmission electron microscopy (TEM, FEI Tecnai G2 F20) were used to observe the powder morphology.

2.3. Electrochemical performance tests

Electrochemical performance evaluations were carried out with CR2025 coin cells in the voltage range of 2.0–4.8 V. For the fabrication of the positive electrode, 320 mg of the as-synthesized materials powder was mixed with 40 mg of conductive additive Super P and 40 mg of binder polyvinylidenedifluoride (PVDF). The above mixture was made into slurry in NMP and coated onto smooth aluminum used as the current collector foil using doctor blade technique. The coated aluminum foil was allowed to dry overnight at 120 °C in a vacuum oven. The coated foil was roller pressed to better adhere the material to the current collector. The cathodes were punched as circular discs from the foil. Lithium foil was used as the negative electrode and Celgard 2400 membrane was used as the separator. The electrolyte was 1 M $LiPF_6$ dissolved in a mixture of ethylene carbonate (EC) and dimethyl carbonate (DMC) with volume ratio 1:1. The cells were assembled inside an argon-filled glove box. The cells were cycled galvanostatically at 25 mA g^{-1} (~0.1 C) between 2.0 and 4.8 V vs. Li^+/Li.

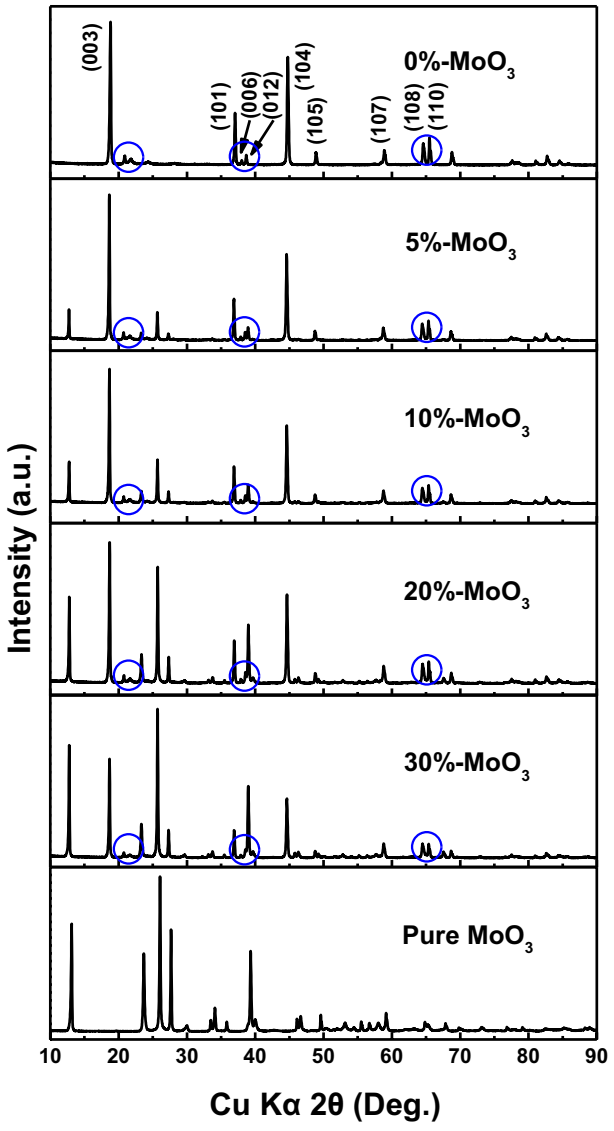

Fig. 1. XRD patterns of MoO_3 and $Li[Li_{0.2}Mn_{0.54}Ni_{0.13}Co_{0.13}]O_2$ composited with various MoO_3 contents.

3. Results and discussion

Fig. 1 shows the XRD patterns of MoO_3 and $Li[Li_{0.2}Mn_{0.54}Ni_{0.13}Co_{0.13}]O_2$ composited with various MoO_3 contents. The diffraction peaks of pure $Li[Li_{0.2}Mn_{0.54}Ni_{0.13}Co_{0.13}]O_2$ can be indexed based on a layered hexagonal a-$NaFeO_2$ structure with a space group of R-3m, except for the weak super lattice reflections

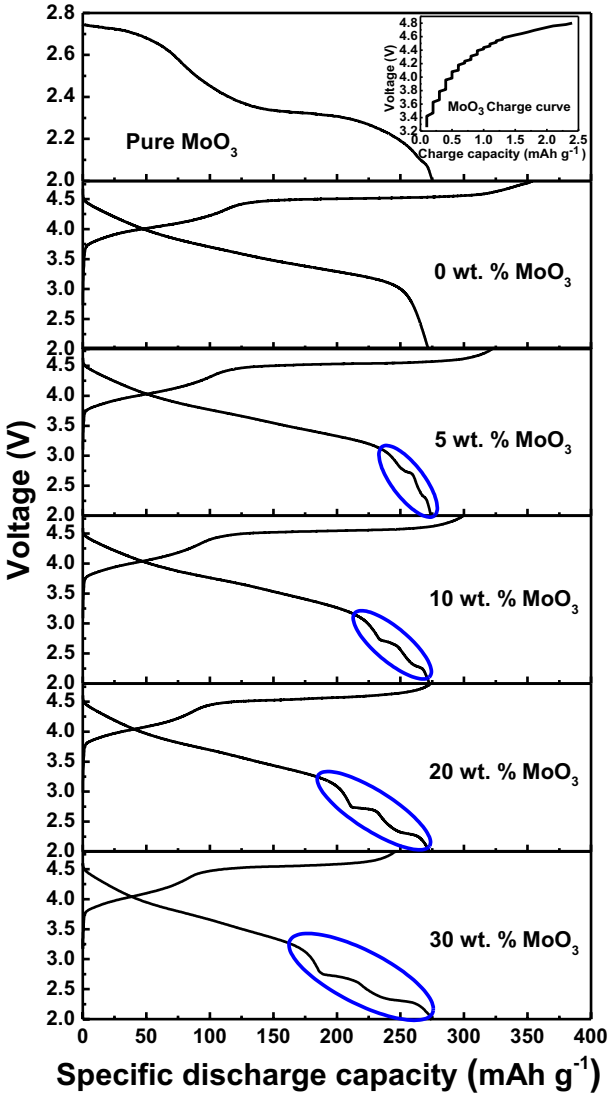

Fig. 2. First charge–discharge profiles of MoO_3 and $Li[Li_{0.2}Mn_{0.54}Ni_{0.13}Co_{0.13}]O_2$ composited with various MoO_3 contents.

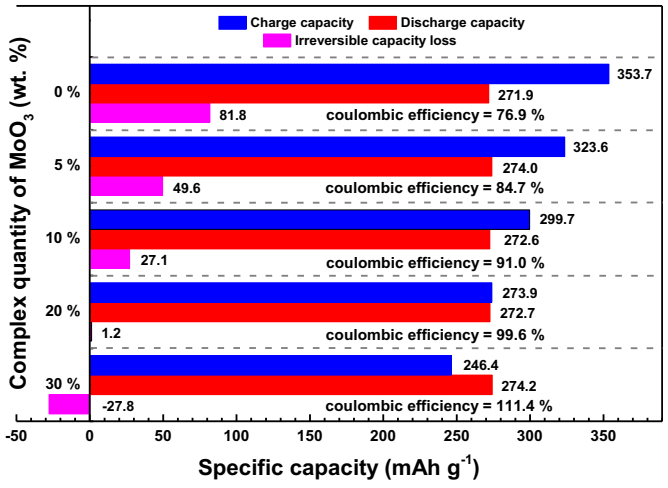

Fig. 3. Variations of the charge capacity, discharge capacity and irreversible capacity loss of $Li[Li_{0.2}Mn_{0.54}Ni_{0.13}Co_{0.13}]O_2$ composited with various MoO_3 contents.

peaks present between 20 and 25°. These weak reflection peaks are caused by the super lattice ordering of Li and Mn in the transition metal layers for the component Li_2MnO_3 ($Li[Li_{1/3}Mn_{2/3}]O_2$) which can be ascribed to the monoclinic phase with a space group of C2/m [6,25–27]. Another observation in the diffraction peaks of pure Li $[Li_{0.2}Mn_{0.54}Ni_{0.13}Co_{0.13}]O_2$ is the clear separation of the (006)/(012) and (018)/(110) peaks, indicating the formation of a well-crystallized layered structure [28].

The diffraction peaks of pure MoO_3 are consistent with JCPDS card: 47-1320, corresponding to orthorhombic crystal system with a space group of P21/m. With the increase in the addition content of MoO_3, the major reflections of the composites still belongs to the pure $Li[Li_{0.2}Mn_{0.54}Ni_{0.13}Co_{0.13}]O_2$ (blue rings). The intensity of the characteristic peaks which belong to pure $Li[Li_{0.2}Mn_{0.54}Ni_{0.13}Co_{0.13}]O_2$ become weaker, and the intensity of the characteristic peaks which belong to pure MoO_3 become stronger.

In order to investigate the electrochemical performance of as-prepared samples, the charge/discharge profiles of the composites were carried out with a R2025 coin-type half-cell employing Li metal as the negative electrode at room temperature in the voltage range between 2.0 and 4.8 V vs. Li/Li^+. Fig. 2 shows the charge–discharge voltage profiles of the composites with different MoO_3 contents at a current density of 25 mA g^{-1} (~0.1 C).

As can be seen from Fig. 2, the first charge curves of all the composites are also composed of a sloping region below 4.5 V and a long plateau region above 4.5 V. The sloping region (3.8 V ~ 4.5 V) is attributed to the extraction of Li^+ ions from the lithium layer. At the same time, the Ni^{2+} and Co^{3+} oxidize to Ni^{4+} and Co^{4+}, respectively. The subsequent long irreversible voltage plateau is around 4.5 V, which beyond the formal oxidation potential of Ni^{2+} to Ni^{4+} and Co^{3+} to Co^{4+}. It is assigned to the simultaneous removal of Li^+ and O^{2-} (as Li_2O) from the lattice of Li_2MnO_3 ($Li[Li_{1/3}Mn_{2/3}]O_2$) component [6,14,16,17]. During the oxygen loss plateau, the component Li_2MnO_3 is activated to form MnO_2-like component and thus the material can deliver higher discharge capacity during the subsequent discharge process. The ideal two-step process during charge can be expressed by reactions (1) and (2). In the first cycle, the discharge capacity of pure $Li_{1.2}Mn_{0.54}Ni_{0.13}Co_{0.13}O_2$ is as high as 271.9 mAh g^{-1}. It is higher than the theoretical capacity of 122.6 mAh g^{-1} based on $Li_{1.2}Mn_{0.54}Ni_{0.13}Co_{0.13}O_2$ according to the reaction of Ni^{2+} to Ni^{4+} and Co^{3+} to Co^{4+}. It is impossible to reintroduce oxygen into the structure on the subsequent discharge, so the higher charge–discharge capacity may be due to the electrochemical activation of Li_2MnO_3 [13]. The ideal process during discharge can be expressed by reaction (3). Based on the above, the theoretical discharge capacity of $Li_{1.2}Mn_{0.54}Ni_{0.13}Co_{0.13}O_2$ is 251.4 mAh g^{-1}. However, the discharge capacity measured by our experiment is larger than 251.4 mAh g^{-1}. Although the precise reasons for the anomalous behavior of $xLi_2MnO_3\cdot(1-x)LiMO_2$ electrodes have not yet been determined, the excess capacity has been attributed tentatively to capacitive effects, electrolyte-related phenomena and possible electronic contributions from the oxygen ions [29].

$$xLi_2MnO_3\cdot(1-x)LiMO_2 \rightarrow xLiMnO_3\cdot(1-x)MO_2 + (1-x)Li \quad (1)$$

$$xLi_2MnO_3\cdot(1-x)MO_2 \rightarrow xMnO_2\cdot(1-x)MO_2 + xLi_2O \quad (2)$$

$$xMnO_2\cdot(1-x)MO_2 + Li \rightarrow xLiMnO_2\cdot(1-x)LiMO_2 \quad (3)$$

As seen in Fig. 2, after compositing with MoO_3, there is an obvious discharge region below 3.0 V (blue ovals in web version). It is in accordance with the discharge of pure MoO_3. With increasing

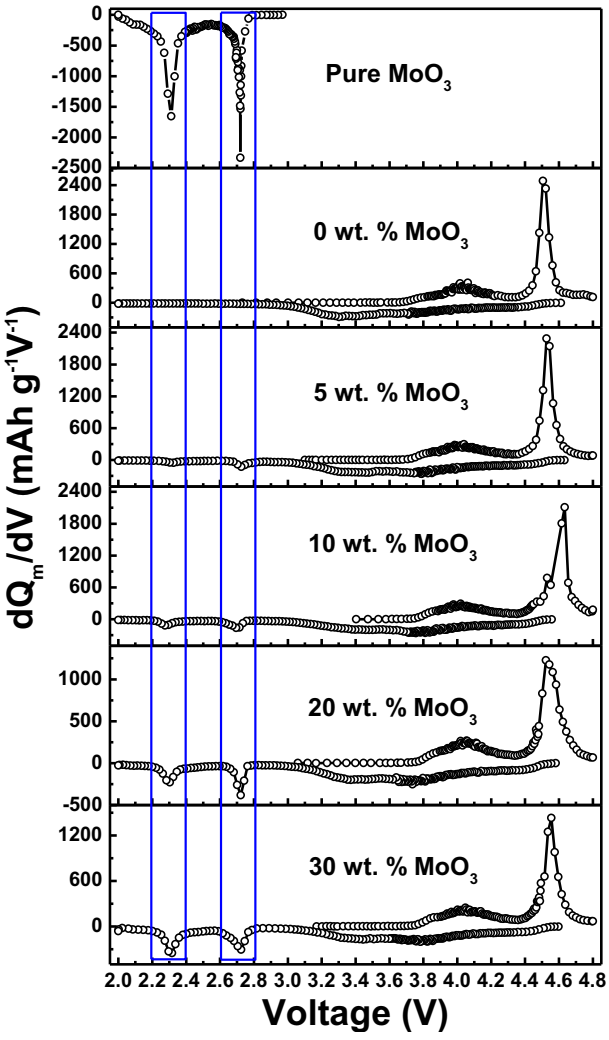

Fig. 4. The differential specific gravimetric capacity vs. voltage (dQ_m/dV) curves of MoO_3 and $Li[Li_{0.2}Mn_{0.54}Ni_{0.13}Co_{0.13}]O_2$ composited with various MoO_3 contents.

MoO_3 content, the charge capacity decreases while the discharge capacity has almost no change and the irreversible capacity loss in the first cycle decreases.

Fig. 3 shows the first charge, discharge capacity, coulombic efficiency value and the irreversible capacity loss of different samples in the first cycle. With increasing MoO_3 content from 0 wt.% to 20 wt.%, the first-cycle irreversible capacity loss of the Li $[Li_{0.2}Mn_{0.54}Ni_{0.13}Co_{0.13}]O_2$–$MoO_3$ composite decreases from 81.8 mAh g^{-1} to 1.2 mAh g^{-1}. 27.8 mAh g^{-1} more capacity is obtained during discharge than during charge when 30 wt.% MoO_3 is reached in the composite sample. With the increase of the MoO_3 addition content (from 0 wt.% to 30 wt.%), the charge capacity of the composite decreases obviously (from 353.7 mAh g^{-1} to 246.4 mAh g^{-1}), while the discharge capacity of the composite has almost no change in the first cycle (from 271.9 mAh g^{-1} to 274.2 mAh g^{-1}).

In order to further understand the reaction in the first charge–discharge process, the differential specific gravimetric capacity vs. voltage (dQ_m/dV) curves of MoO_3 and $Li[Li_{0.2}Mn_{0.54}Ni_{0.13}Co_{0.13}]O_2$–$MoO_3$ composites are discussed. It was measured at a constant current density of 25 mA g^{-1} (~0.1 C) in the range from 2.0 to 4.8 V at room temperature. As shown in Fig. 4, there are two obvious oxidation peaks at the initial charge curve of all the $Li[Li_{0.2}Mn_{0.54}Ni_{0.13}Co_{0.13}]O_2$–$MoO_3$ samples in the first charging progress.

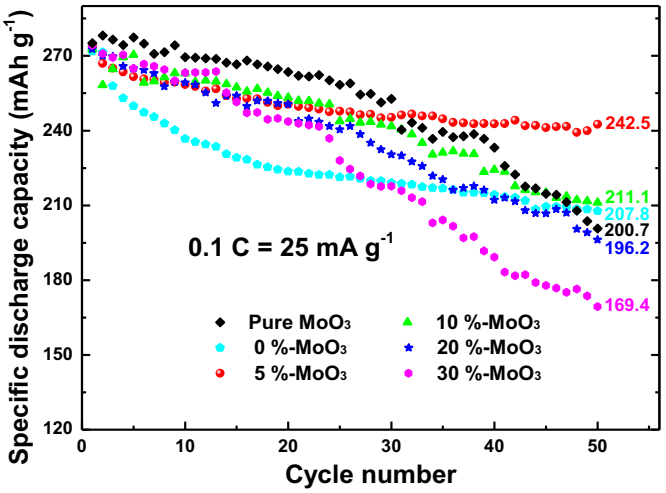

Fig. 5. Comparison of the cycling stability of MoO_3 and $Li[Li_{0.2}Mn_{0.54}Ni_{0.13}Co_{0.13}]O_2$ composited with various MoO_3 contents.

The oxidation peak at around 4.0 V is due to the oxidation of Ni and Co ions of the $Li[Ni_{1/3}Mn_{1/3}Co_{1/3}]O_2$ component. The sharp oxidation peak at around 4.5 V is attributed to the removal of Li_2O from the $Li[Li_{1/3}Mn_{2/3}]O_2$ component. This sharp oxidation peak disappears in the subsequent cycles. In the first discharging progress, another two distinct reduction peaks (blue boxes in web version) appear resulting from compositing with MoO_3, which was consistent with the reduction peaks of MoO_3. The decrease in irreversible capacity loss is due to the ability to insert the lithium back into the lithium-free host MoO_3 in the composite cathodes. These observations are consistent with previous findings with the composite cathodes consisting of layered $Li[Li_{0.2}Mn_{0.54}Ni_{0.13}Co_{0.13}]O_2$ and other lithium-free insertion hosts, such as V_2O_5, $Li_4Mn_5O_{12}$, and LiV_3O_8 [22,23].

Fig. 5 compares the cycling stability of the layered Li $[Li_{0.2}Mn_{0.54}Ni_{0.13}Co_{0.13}]O_2$, MoO_3, and $Li[Li_{0.2}Mn_{0.54}Ni_{0.13}Co_{0.13}]O_2$–$MoO_3$ composites at 25 mA g^{-1} (~0.1C). Compared with pristine material $Li[Li_{0.2}Mn_{0.54}Ni_{0.13}Co_{0.13}]O_2$, the composite cathodes Li $[Li_{0.2}Mn_{0.54}Ni_{0.13}Co_{0.13}]O_2$–$MoO_3$ exhibits a better cycling stability before 20 cycles. However, the discharge capacity of the composite cathodes decreases very fast after the 20th cycle except the composite cathodes with 5 wt.% MoO_3. The composite cathodes with 5 wt.% MoO_3 show the best capacity retention than other composites with a capacity retention 242.5 mAh g^{-1} after 50 cycles. However, with increasing MoO_3 content, the capacities fade of the composite cathodes becomes more serious and even worse than 207.8 mAh g^{-1} of the pristine layered oxide after 50 cycles.

In order to investigate the reasons for changes of as-prepared samples, the SEM and TEM analysis were performed and the images are shown in Fig. 6. Obviously, the bare $Li[Li_{0.2}Mn_{0.54}Ni_{0.13}Co_{0.13}]O_2$ powders consist of the nanocrystallines with a size distribution of 100–300 nm, and the surface of the bare Li $[Li_{0.2}Mn_{0.54}Ni_{0.13}Co_{0.13}]O_2$ particles is smooth (Fig. 6(a)). After composited with MoO_3 (5 wt.%), no obvious change of the particles shape and size is observed. However, the surface of the Li $[Li_{0.2}Mn_{0.54}Ni_{0.13}Co_{0.13}]O_2$–$MoO_3$ (5 wt.%) particles get rough (Fig. 6(b)). Under close magnification, as shown in Fig. 6(c), there is a compact amorphous coating layer with a thickness of about 3–4 nm on the surface of $Li[Li_{0.2}Mn_{0.54}Ni_{0.13}Co_{0.13}]O_2$ particles. The coating layer is believed to be MoO_3 layer, which form in the high-energy ball milling treatment process.

In order to better understand the significance of the compact amorphous MoO_3 coating layer introduced by the high-energy ball

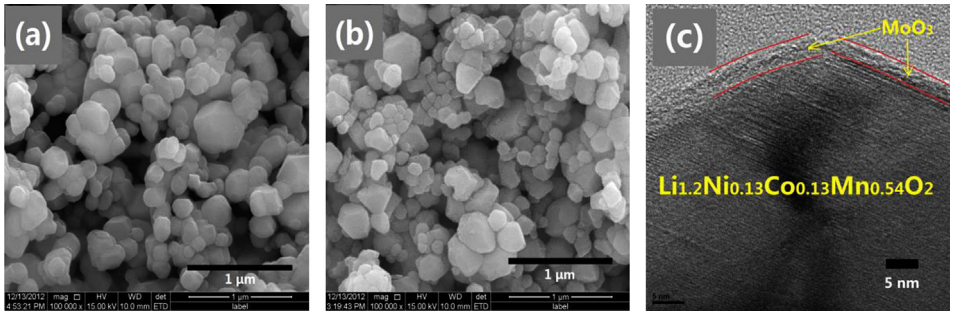

Fig. 6. (a) SEM image of $Li[Li_{0.2}Mn_{0.54}Ni_{0.13}Co_{0.13}]O_2$. (b)SEM image of $Li[Li_{0.2}Mn_{0.54}Ni_{0.13}Co_{0.13}]O_2$–$MoO_3$ (5 wt.%). (c) TEM image of $Li[Li_{0.2}Mn_{0.54}Ni_{0.13}Co_{0.13}]O_2$–$MoO_3$ (5 wt.%).

milling treatment process, the electrochemical performances of two series (series by ball milling and series by direct mixing) as-prepared samples with different amounts of MoO_3 were measured. Fig. 7 shows the cycle performances of two series (series by ball milling and series by direct mixing) as-prepared samples with different amounts of MoO_3. By comparison, it is shown that the series by ball milling have much better cycling ability than the series by direct mixing. The better cycling ability of the series by ball milling is possibly due to the compact amorphous MoO_3 coating layer on the surface of $Li[Li_{0.2}Mn_{0.54}Ni_{0.13}Co_{0.13}]O_2$ particles, which can suppress the side reactions between the active cathode materials and the electrolyte. Fig. 8 shows the first cycle columbic efficiency of two series (series by ball milling and series by direct mixing) as-prepared samples with different amounts of MoO_3. As seen from Fig. 8, the first cycle columbic efficiency of the series by ball milling is higher than the series by direct mixing as well. Therefore, it can be concluded that the amorphous MoO_3 coating layer is of significance in improving the cycling ability of these cathodes, as well as the first cycle columbic efficiency.

For $LiNi_{1/3}Co_{1/3}Mn_{1/3}O_2$ cathode, the capacity loss can be ascribed to four factors: (1) lattice volume in the charge/discharge process; (2) cation mixing; (3) transition metal ion dissolution; (4) side reaction between electrode and electrolyte [28,30,31]. For Li-rich layered oxides (Li_2MnO_3–$LiMO_2$), two factors have been demonstrated to affect the cycling stability [32–35]: (1) the dissolution of the metal ions, especially the manganese ion during the charge–discharge process; (2) the Jahn–Teller distortion during cycling. Surface coating can effectively improve the cyclic performance of the cathode materials [36]. The MoO_3 coating layer on the surface of particles, acting as a protective layer, which can decrease the direct contact between the electrolyte and electrode. It can effectively suppress the active material reacting with electrolyte and the dissolution of transition metal elements during cycling.

Through investigating the surface of the as-prepared samples, there are two reasons of the phenomenon as described in Fig. 5: (1) as it is well known, the capacity fading of lithium-rich cathode materials is a complex phenomenon related to both the bulk structure and interface stability. The better cycling stability of the composite cathodes before 20 cycles is related to the enhanced interface stability because the MoO_3 coating layer on the surface formed in the compound procedures. (2) With increasing the content of MoO_3, the fast fading of the composite cathodes discharge capacity after the 20th cycle is attributed to the faster capacity fade of MoO_3. The MoO_3 obtained by decomposing $(NH_4)_6Mo_7O_{24}\cdot 4H_2O$ may not have the optimum characteristics to show good cycling stability. Thus, too much MoO_3 contents composited with $Li[Li_{0.2}Mn_{0.54}Ni_{0.13}Co_{0.13}]O_2$ results in bad cycling stability.

4. Conclusions

The large first-cycle irreversible capacity loss of $Li[Li_{0.2}Mn_{0.54}Ni_{0.13}Co_{0.13}]O_2$ can be eliminated by a simple surface treatment with MoO_3 through high-energy ball milling. The elimination of the irreversible capacity loss is due to the lithium-free insertion host

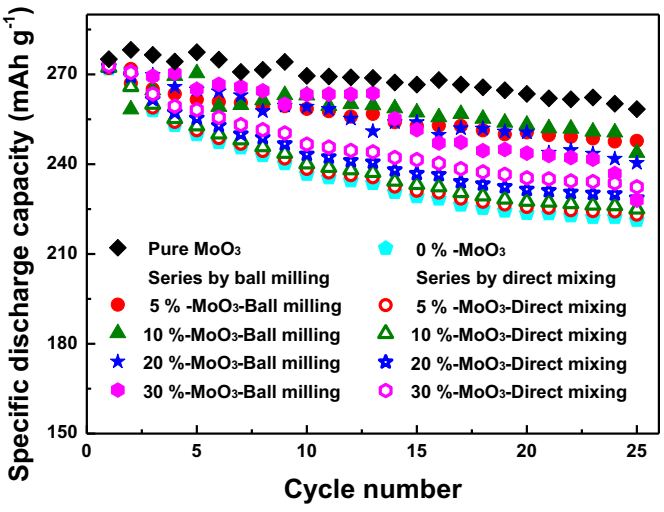

Fig. 7. The cycle performances of the two series as-prepared samples with different amounts of MoO_3.

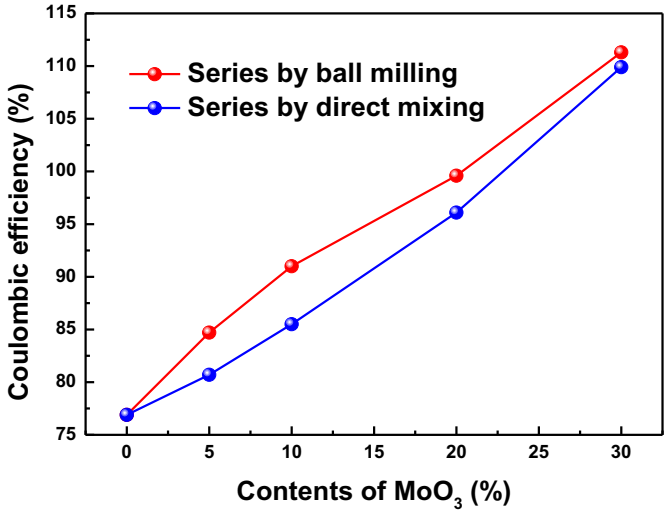

Fig. 8. The first cycle columbic efficiency of the two series as-prepared samples with different amounts of MoO_3.

MoO_3 which can accommodate the lithium ions that could not insert back into the layered lattice after the first charge. With the increase of the addition content of MoO_3, the charge capacity of the composite decreased obviously, while the discharge capacity of the composite had almost no change in the first cycle. The Li$[Li_{0.2}Mn_{0.54}Ni_{0.13}Co_{0.13}]O_2$ composited with an optimum MoO_3 content of 20 wt.% exhibits a high discharge capacity of 273.9 mAh $g^{-1}$and a little irreversible capacity loss of 1.2 mAh g^{-1}. The Li$[Li_{0.2}Mn_{0.54}Ni_{0.13}Co_{0.13}]O_2$ composited with 5 wt.% MoO_3 exhibits a good cycle ability with the discharge capacity of 242.5 mAh g^{-1} after 50 cycles, which could due to a nano-sized MoO_3 layer coated on the Li$[Li_{0.2}Mn_{0.54}Ni_{0.13}Co_{0.13}]O_2$ surface by the high-energy ball milling process. However, with the increase in the addition content of MoO_3, the cycling stability of the composite cathodes Li$[Li_{0.2}Mn_{0.54}Ni_{0.13}Co_{0.13}]O_2$–$MoO_3$ decreases.

Acknowledgements

This work was funded by the Key National Basic Research and Development Program of China (2009CB220100), National Natural Science Foundation of China (51102018, 21103011) and National High-Tech Research, Development Program of China (2011AA11A235, SQ2010AA1123116001) and BIT Scientific and Technological Innovation Project (2013CX01003).

References

[1] J.-H. Ju, K.-S. Ryu, J. Alloys Compd. 509 (2011) 7985.
[2] B. Scrosati, J. Garche, J. Power Sources 195 (2010) 2419.
[3] J.M. Tarascon, M. Armand, Nature 414 (2001) 359.
[4] S. Venkatraman, Y. Shin, A. Manthiram, Electrochem. Solid-State Lett. 6 (2003) A9.
[5] R.V. Chebiam, F. Prado, A. Manthiram, Chem. Mater. 13 (2001) 2951.
[6] M.M. Thackeray, S. Kang, C.S. Johnson, J.T. Vaughey, R. Benedek, S.A. Hackney, J. Mater. Chem. 17 (2007) 3112.
[7] B. Ammundsen, J. Paulsen, Adv. Mater. 13 (2001) 943.
[8] Z. Lu, L.Y. Beaulier, R.A. Donaberger, C.L. Thomas, J.R. Dahn, J. Electrochem. Soc. 149 (2002) A778.
[9] S.H. Kang, K. Amine, J. Power Sources 124 (2003) 533.
[10] J. Jiang, K.W. Eberman, L.J. Krause, J.R. Dahn, J. Electrochem. Soc. 152 (2005) A1879.
[11] L.Q. Zhang, K. Takada, N. Ohta, K. Fukuda, T. Sasaki, J. Power Sources 146 (2005) 598.
[12] M.M. Thackeray, C.S. Johnson, J.T. Vaughey, N. Li, S.A. Hackney, J. Mater. Chem. 15 (2005) 2257.
[13] Z.H. Lu, J.R. Dahn, J. Electrochem. Soc. 149 (2002) A815.
[14] A.R. Armstrong, M. Holzapfel, P. Novak, C.S. Johnson, S. Kang, M.M. Thackeray, P.G. Bruce, J. Am. Chem. Soc. 128 (2006) 8694.
[15] Y. Wu, A. Manthiram, Electrochem. Solid-State Lett. 9 (2006) A221.
[16] J. Liu, Q. Wang, B. Reeja-Jayan, A. Manthiram, Electrochem. Commun. 12 (2010) 750.
[17] C.S. Johnson, J.-S. Kim, C. Lefief, N. Li, J.T. Vaughey, M.M. Thackeray, Electrochem. Commun. 6 (2004) 1085.
[18] Y. Wu, A.V. Murugan, A. Manthiram, J. Electrochem. Soc. 155 (2008) A635.
[19] Q.Y. Wang, J. Liu, A.V. Murugan, A. Manthiram, J. Mater. Chem. 19 (2009) 4965.
[20] J.M. Zheng, J. Li, Z.R. Zhang, X.J. Guo, Y. Yang, Solid-State Ionics 179 (2008) 1794.
[21] J.-S. Kim, C.S. Johnson, J.T. Vaughey, M.M. Thackeray, J. Power Sources 153 (2006) 258.
[22] J. Gao, J. Kim, A. Manthiram, Electrochem. Commun. 11 (2009) 84.
[23] J. Gao, A. Manthiram, J. Power Sources 191 (2009) 644.
[24] F. Wu, N. Li, Y.F. Su, H.Q. Lu, L.J. Zhang, R. An, Z. Wang, L.Y. Bao, S. Chen, J. Mater. Chem. 22 (2012) 1489.
[25] J. Liu, B. Reeja-Jayan, A. Manthram, J. Phys. Chem. C 114 (2010) 9528.
[26] J. Liu, A. Manthiram, J. Mater. Chem. 20 (2010) 3961.
[27] B. Zhang, G. Chen, P. Xu, C.C. Li, J. Power Sources 176 (2008) 325.
[28] K.M. Shaju, G.V. SubbaRao, B.V.R. Chowdari, Electrochim. Acta 48 (2002) 145.
[29] C.S. Johnson, N. Li, C. Lefief, M.M. Thackeray, Electrochem. Commun. 9 (2007) 787.
[30] G.-H. Kim, J.-H. Kim, S.-T. Myung, C.S. Yoon, Y.-K. Sun, J. Electrochem. Soc. 152 (2005) A1707.
[31] S.-T. Myung, K. Izumi, S. Komaba, Y.-K. Sun, H. Yashiro, N. Kumagai, Chem. Mater. 17 (2005) 3695.
[32] A. Ito, D. Li, Y. Sato, M. Arao, M. Watanabe, M. Hatano, H. Horie, Y. Ohsaw, J. Power Sources 195 (2010) 567.
[33] J. Park, J.H. Seo, G. Plett, W. Lu, A.M. Sastry, Electrochem. Solid-State Lett. 14 (2011) A14.
[34] D.H. Jang, Y.J. Shin, S.M. Oh, J. Electrochem. Soc. 143 (1996) 2204.
[35] M. Wohlfahrt-Mehrens, C. Vogler, J. Garche, J. Power Sources 127 (2004) 58.
[36] C. Li, H.P. Zhang, L.J. Fu, H. Liu, Y.P. Wu, E. Rahm, R. Holze, H.Q. Wu, Electrochim. Acta 51 (2006) 3872.